Oxide Complexes in Alkali–Alkaline-Earth Chloride Melts

S. Boghosian,* Aa. Godø, H. Mediaas, W. Ravlo and T. Østvold†

Institute of Inorganic Chemistry, The Norwegian Institute of Technology, N-7034 Trondheim, Norway

Boghosian, S., Godø, Aa., Mediaas, H., Ravlo, W. and Østvold, T., 1991. Oxide Complexes in Alkali–Alkaline-Earth Chloride Melts. – Acta Chem. Scand. 45: 145–157.

The solubilities of alkaline-earth oxides in alkali–alkaline-earth chloride, NaCl–MCl_2, melts are presented. The oxide solubility increases markedly with the MCl_2 concentration and with increasing size of the alkaline-earth ion. The enhanced solubility of the oxide is explained through the reaction

$$m\mathrm{MCl_2(l)} + n\mathrm{MO(s)} = \mathrm{M_{m+n}O_nCl_{2m}(l)}$$

In NaCl–MCl_2 containing 25 mol % MCl_2 the MO solubilities at 850 °C are $x_{MgO} = 6\times10^{-5}$, $x_{CaO} = 10^{-3}$–10^{-4} and $x_{SrO} = 0.039$, respectively. In the $BaCl_2$ system the BaO/$BaCl_2$ molar ratio at saturation is 1. The oxochlorocomplexes formed in these melts are further justified through cryoscopic measurements showing an increasing melting point of a binary NaCl–MCl_2 melt when oxide is added. Model calculations in combination with the two sets of experimental data indicate that the M/O ratios for the different complexes are Mg_2O, Ca_3O, Ca_4O, Sr_3O, Sr_4O, Ba_3O and Ba_4O_2. The formation constants for neutral complexes based on the reactions

$$(m + n)\mathrm{M^{2+}} + n\mathrm{O^{2-}} + 2m\mathrm{Cl^-} = \mathrm{M_{m+n}O_nCl_{2m}}$$

are very large.

In technical melts for Mg electrolysis the MgO solubility is very small (in the ppm region). Even if BaO dissolves readily in NaCl–$BaCl_2$ melts the solubility of BaO is very small in $MgCl_2$-containing melts, since BaO(s) reacts with $MgCl_2$(l) to form $BaCl_2$(l) and MgO(s).

The physicochemical properties of the magnesium chloride electrolyte are of great significance in technical magnesium electrolysis. Properties such as the density,[1,2] conductivity[3] and viscosity[4] of the electrolyte and interphasial properties[5] of the melt and the liquid metal are of significant importance for the current and energy efficiency of the process. The solubility of the reaction products, Mg and Cl_2, in the electrolyte is also important for an evaluation of the current efficiency of the electrochemical process.[8–11] Interphasial properties of the Mg electrolyte interphase may depend significantly on the oxide concentrations of the liquid bath.[12]

The influence of oxide impurities in the melt on the magnesium solubility and on the degree of magnesium metal dispersion (for Mg particles with $d<0.1$ mm) has been studied in a few papers.[8,12] The motivations of these studies were problems associated with high oxide contents in the electrolyte during magnesium production. The very small MgO solubility in halide melts[13,14] supports the fact that Mg^{2+}–O^{2-} interactions are very strong. This also indicates possible Mg–O–Cl complex formation in $MgCl_2$–alkali chloride melts containing oxide impurities.

In modern electrolyzers for magnesium production the metal is collected above the melt surface, the density of the melt thus being larger than the density of the metal. The compositions of the electrolytes are therefore somewhat restricted, and are usually made up of a combination of $MgCl_2$, NaCl and KCl with or without $CaCl_2$ or $BaCl_2$.[15a] The effect of these additives on the rate of Mg sludge formation has been extensively studied.[15b] However, little is known about the possible Mg–O–Cl complexes which may form in such melts and in this way increase the MgO solubility. Combes *et al.*[16] used calcia-stabilized zirconia electrodes to determine the O^{2-} ion concentration in a $MgCl_2$–NaCl–KCl solution at 727 °C with varying BaO additions. From their experimental data the equilibrium constants for reactions (1) and (2) were determined to be $K_1 = x_{Mg_2O^{2+}}x_{O^{2-}}^{-1}x_{Mg^{2+}}^{-2} = 5.06\times10^{11}$ and $K_2 = x_{O^{2-}}^{-1}x_{Mg_2O^{2+}}^{-1} = 7.14\times10^{10}$. The solubility product of MgO in the equimolar NaCl–KCl mixture at 1000 K was $K_{sp}(MgO) = x_{Mg^{2+}}^{-1}x_{O^{2-}}^{-1} =$

$$2\mathrm{Mg^{2+}} + \mathrm{O^{2-}} \rightarrow \mathrm{Mg_2O^{2+}} \quad (1)$$

$$\mathrm{Mg_2O^{2+}} + \mathrm{O^{2-}} \rightarrow 2\mathrm{MgO(s)} \quad (2)$$

* Present address: Institute of Chemical Engineering and High Temperature Chemical Processes, University of Patras, P.O. Box 1239, GR-26110 Patras, Greece.

† To whom correspondence should be addressed.

$(K_1K_2)^{-1/2} = 5.3\times10^{-12}$. The solubilities of the other alkaline-earth oxides in the equimolar NaCl–KCl melt are low but are considerably larger than that of MgO and increase in the sequence MgO, CaO, SrO, BaO.[16,17] In alkaline-earth chloride-rich melts, however, the solubilities of the corresponding oxides are considerable. Barium chloride may dissolve as much as 20 mol % BaO at 1000 °C.[18] The solubilities at 1000 °C of SrO in $SrCl_2$[18] and of CaO in $CaCl_2$[19] are of the order of 30 and 20 mol %, respectively. The large differences in the solubilities of the oxides indicate different dissolution mechanisms of the oxides in the alkali chloride and alkaline-earth chloride melts, respectively.

The phase diagrams of the binary systems MgF_2–MgO (CaO and Al_2O_3) have recently been published.[20] The observed freezing-point depression of MgF_2(l) when adding the oxides MgO and CaO supports the assumption of Mg_2O^{2+} ion formation and that the cations Mg^{2+}, Ca^{2+} and Mg_2O^{2+} mix ideally at low oxide additions.

The motivation for the present paper is, for the above-mentioned reasons, twofold. First, we wish to establish the oxide solubility and the mechanism of oxide dissolution in melts of interest for technical magnesium electrolysis. Secondly, we wish to explain the dissolution mechanism of alkaline-earth oxides in binary molten mixtures of some of the corresponding alkaline-earth halides with NaCl. To accomplish this we have measured the equilibrium oxide concentrations in MO–MCl_2–NaCl (M = Mg, Ca, Sr and Ba) as a function of temperature and composition. In systems with high oxide solubility (M = Ca, Sr and Ba) we have further measured the liquidus temperatures in the NaCl(s) phase field of the calcium, strontium and barium ternary systems.

Principles

Since the solubilities of the alkaline-earth oxides in the chloride and fluoride melts are dependent on the concentration of the alkaline-earth ions present in such melts, we may assume that reactions such as eqn. (3) are responsible

$$m\mathrm{MCl_2(l)} + n\mathrm{MO(s)} = \mathrm{M_{m+n}O_nCl_{2m}(l)} \quad (3)$$

for the enhanced oxide solubilities observed with increasing M^{2+} concentrations. In an evaluation of experimental data it is often useful to have a model of the investigated system. In the present case eqn. (3) predicts that the equilibrium mole fractions of the oxide complex will be proportional to the activity of MCl_2 in the liquid mixture to the mth power as long as the oxide solubilities are low. The freezing points of the ternary mixture in the phase field where NaCl(s) is precipitated are related to the activity of NaCl. By introducing binary MCl_2 and NaCl activities into the ternary system at low oxide solubilities we are able to compare experimental solubilities and freezing points with model predictions.

Oxide solubility studies. When the solubility of an alkaline-earth oxide in NaCl–MCl_2 (M = Mg, Ca, Sr, Ba) is small, Henry's law [eqn. (4)] is valid for the oxide complex $M_{m+n}O_nCl_{2m}$ where k is the Henry's law constant. Then, the equilibrium constant K_3 for eqn. (3) is given by eqns. (5) and (6).

$$a_{\mathrm{M_{m+n}O_nCl_{2m}}} = kx_{\mathrm{M_{m+n}O_nCl_{2m}}} \quad (4)$$

$$K_3 = \frac{a_{\mathrm{M_{m+n}O_nCl_{2m}}}}{a^m_{\mathrm{MCl_2}}} = k\,\frac{x_{\mathrm{M_{m+n}O_nCl_{2m}}}}{a^m_{\mathrm{MCl_2}}} \quad (5)$$

$$x_{\mathrm{M_{m+n}O_nCl_{2m}}} = K_3k^{-1}\,a^m_{\mathrm{MCl_2}} \quad (6)$$

$$x_{\mathrm{MCl_2}} = \frac{n^\circ_{\mathrm{MCl_2}} - (m/n)n^\circ_{\mathrm{MO}}}{n^\circ_{\mathrm{NaCl}} + n^\circ_{\mathrm{MCl_2}} - [(m-1)/n]n^\circ_{\mathrm{MO}}} \quad (7)$$

$$x_{\mathrm{M_{m+n}O_nCl_{2m}}} = \frac{(1/n)n^\circ_{\mathrm{MO}}}{n^\circ_{\mathrm{NaCl}} + n^\circ_{\mathrm{MCl_2}} - [(m-1)/n]n^\circ_{\mathrm{MO}}} \quad (8)$$

The equilibrium mole fractions of MCl_2 and $M_{m+n}O_nCl_{2m}$ can be obtained from eqns. (7) and (8), derived using the appropriate mass balance equations, where n°_{NaCl} and $n^\circ_{\mathrm{MCl_2}}$ are the initial numbers of moles of NaCl and MCl_2 (M = Mg, Ca, Sr and Ba), and n°_{MO} is the number of moles of alkaline-earth oxide dissolved in the melt. It is assumed that all the dissolved oxide is being used for complex formation. This assumption may be questionable for BaO additions to the $BaCl_2$–NaCl system when $x_{\mathrm{BaCl_2}}$ is small. This problem will be discussed later.

Values for m and n may be obtained by comparing experimental data and model calculations, since eqn. (6) predicts that the mole fraction of the oxide complex should be proportional to $a^m_{\mathrm{MCl_2}}$. The value of n, however, is not easy to obtain at low oxide solubilities using eqns. (6)–(8), since $x_{\mathrm{MCl_2}}$ does not vary much with varying oxide solubility.

Cryoscopic studies. The cryoscopic method used in the present study is similar to the one described by Ratkje[21–23] and will only briefly be discussed here. The starting melt is a mixture of sodium chloride and alkaline-earth chloride with known composition. Alkaline-earth oxide is added in small increments and the effect on the freezing point of the melt, from which NaCl is crystallizing, is recorded. According to eqn. (3) the number of "foreign species" in the melt is reduced by $m-1$ when MO is added. Accordingly one should expect an elevation of the freezing point when $m>1$.

$$T_{\mathrm{f}} = \frac{T^\circ_{\mathrm{f,NaCl}}\,\Delta H^\circ_{\mathrm{f,NaCl}}}{\Delta H^\circ_{\mathrm{f,NaCl}} - RT^\circ_{\mathrm{f,NaCl}}\ln a_{\mathrm{NaCl}}} \quad (9)$$

$$a_{\mathrm{NaCl}} = x_{\mathrm{Na^+}}x_{\mathrm{Cl^-}} \quad (10)$$

The freezing point temperature is given by eqn. (9), where $T°_{f,NaCl}$ = 800.6 °C, $\Delta H°_{f,NaCl}$ = 28158 J mol^{-1},[24] and a_{NaCl} is the NaCl activity at the liquidus composition. According to the Temkin model,[25] the activity of NaCl in a fused salt solution is given by eqn. (10). In the ideal Temkin mixtures the activity coefficient, γ, is equal to 1. In the present case

$$m\mathrm{MCl_2(l)} + n\mathrm{MO(s)} + p\mathrm{NaCl(l)}$$

$$= \mathrm{M_{m+n}O_nCl_{2m+p}}^{p-}\mathrm{(l)} + p\mathrm{Na^+} \quad (11)$$

deviation from ideality is observed. In the $SrCl_2$–NaCl binary, for example, the measured NaCl activity at T = 1123 K and x_{NaCl} = 0.69 is 0.64, while the ideal activity is 0.69.[26] When oxide is added to the chloride melt, cationic or anionic oxide-containing complexes may form according to reactions such as eqn. (11). For $p<0$ complex cations and for $p>0$ complex anions will form. Since the activity of NaCl is given by eqn. (10), we have to consider both cases in a comparison between experimental liquidus temperatures and those calculated by eqn. (9). In the case of cationic complexes x_{Cl^-} = 1, and the activity of NaCl is given by eqn. (12). In the case of anionic complexes, the activity of NaCl is given by eqn. (13).

$$a_{NaCl} = x_{Na^+}\gamma_{NaCl} = \frac{n°_{NaCl}}{n°_{NaCl} + n°_{MCl_2} - [(m-1)/n]n°_{MO}}\gamma_{NaCl} \quad (12)$$

$$a_{NaCl} = x_{Na^+}x_{Cl^-}\,\gamma_{NaCl}$$

$$= \frac{n°_{NaCl}}{n°_{NaCl} + n°_{MCl_2} - [(m-1)/n]n°_{MO}} \times \frac{n°_{NaCl} + 2n°_{MCl_2} - [(2m+p)/n]n°_{MO}}{n°_{NaCl} + 2n°_{MCl_2} - [(2m+p-1)/n]n°_{MO}}\gamma_{NaCl} \quad (13)$$

Activities obtained using eqns. (12) and (13) are not significantly different at low oxide contents, and we were not able on the basis of our data to distinguish between the two models. In the model calculations presented later in this paper we have for simplicity used eqn. (12).

Experimental

Experiments and handling of salts were carried out in an argon-filled dry box (Vacuum/Atmospheres Corp.) with water and oxygen contents at the 10 ppm level.

Materials. Sodium chloride (Merck, 99.5 %) was dried under vacuum at 400 °C and recrystallized twice in platinum crucibles under an inert atmosphere (N_2). Anhydrous alkaline-earth chlorides were prepared from $MgCl_2·6H_2O$ (Merck, 99 %), $CaCl_2·2H_2O$ (Merck, 99.5 %), $SrCl_2·6H_2O$ (Merck, 99 %) and $BaCl_2·2H_2O$(Merck, 99 %). The anhydrous salts were prepared by dehydration in a stream of HCl(g) or N_2(g) while being heated to 300–500 °C over several days. Dehydrated $MgCl_2$ was vacuum-distilled twice. Dehydrated $CaCl_2$ was zone-refined for 4 days, and $SrCl_2$ and $BaCl_2$ were recrystallized from their respective melts in quartz crucibles in an N_2(g) atmosphere. The level of oxide contamination in the final products was determined by analysis and was found to be at the level of 10, 50, 120 and 150 ppm as alkaline-earth oxide for $MgCl_2$, $CaCl_2$, $SrCl_2$ and $BaCl_2$, respectively. The alkaline-earth oxides were prepared by thermal decomposition of the corresponding carbonates under vacuum at temperatures of 350 °C for $MgCO_3$ (Merck, 99.2 %), 750 °C for $CaCO_3$ (Fluka, 98 %) and 1000 °C for $SrCO_3$ (Merck, 99.8 %) and $BaCO_3$ (Baker, 99.3 %). The purity of the resulting alkaline-earth oxide was routinely checked by measuring the weight loss due to the decomposition reaction $MCO_3(s) \rightarrow MO(s) + CO_2(g)$.

Containers. Several crucible materials, such as alumina, magnesia, platinum, quartz and vitreous carbon, were examined as containers, but none proved to be completely inert. Thus, pure gold was used as the only material in direct contact with the melts. For the MgO-containing melts platinum crucibles could, however, be used owing to the extremely low solubility of this oxide in NaCl–$MgCl_2$ melts.

General procedure. A schematic diagram of the experimental set-up is shown in Fig. 1. Crucibles to be used as melt containers were filled with weighed amounts of salts and placed at the bottom of a quartz container fitted with alumina radiation shields having holes to accommodate the stirring rod, salt charger or sample extraction tube, and thermocouple. The stirring rod was made of Alsint. The thermocouple was contained in an alumina case and placed directly into the melt. Both the stirring rod and the thermocouple case had gold or platinum sheaths around the parts to be immersed in the melt. The entire cell assembly was placed inside the cylindrical core of a Kanthal REH-S wire-wound, water-cooled furnace whose temperature was controlled by a proportional controller. The core of the furnace was constituted of a nickel tube tightly connected to the glovebox. The cell assembly was left open to the box atmosphere.

Oxide solubility studies. Equilibration of molten chloride mixtures with added oxide was carried out in the glove box as described above under an argon atmosphere at 730 and 830 °C in $MgCl_2$-containing melts, and at 850 °C in $CaCl_2$-, $SrCl_2$- and $BaCl_2$- containing melts. Preweighed amounts of sodium chloride, alkaline-earth chloride and alkaline-earth oxide were transferred into a dry and clean gold/platinum crucible. The alkaline-earth oxide was in excess to ensure that the solutions would be saturated. Equilibration times in each NaCl–MCl_2–MO (M = Mg, Ca, Sr, Ba) system were determined in separate experiments in which the oxide content of the molten mixtures was measured as a

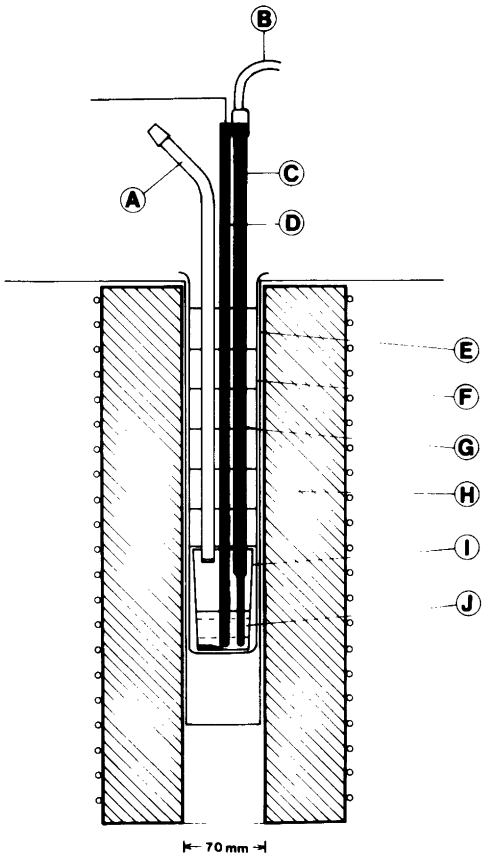

Fig. 1. Experimental set-up for solubility and cryoscopic measurements inside a glove box: (A) silica sampling tube with a silica sinter (porosity 2 or 3) at the end; (B) flexible wire connected to stirring motor; (C) stirrer, alumina rod with Au or Pt casing at the tip; (D) thermocouple, Pt, Pt10Rh or Cr, CrNi in alumina tubing with Au or Pt casing at the tip; (E) nickel tube tightly connected to glovebox; (F) silica cell; (G) alumina radiation shields; (H) furnace; (I) Au or Pt crucible; (J) melt.

function of time. This was done by periodically sampling 3–10 g of the molten mixture by means of a syringe which was coupled to a quartz sampling tube. During the time intervals between two successive samplings the melts were stirred continuously. The sampling tube had a quartz sintered frit (pore size 15–90 μm) at the bottom and was immersed in the melt only during the sampling procedure (1–2 min). Samples were quenched at room temperature and analyzed for oxide content by being dissolved in known amounts of hydrochloric acid, the excess of HCl then being titrated iodometrically. Acid–base titration was used in $BaCl_2$-containing melts owing to the formation of $Ba(IO_3)(s)$ and $Ba_2S_2O_3(s)$ during the iodometric titration. In order to measure the alkaline-earth oxide solubility in NaCl–MCl_2 (M = Mg, Ca, Sr, Ba) melts, each molten mixture was continuously stirred and equilibrated for a sufficient time (up to 60 h). Melt samples were taken and analyzed for oxide content as described above. The composition of the melt could then be changed by further additions of MCl_2 and NaCl through a charging tube positioned just above the melt.

Cryoscopic studies. Cryoscopic measurements were performed under an argon atmosphere by using the experimental set-up as described above (Fig. 1). For each experiment about 60 g of melt was used. The temperature was measured with a Pt–Pt10 % Rh thermocouple; the thermal EMF was recorded using a differential voltmeter (Fluke 809S AB) equipped with a strip-chart recorder.

Molten NaCl–MCl_2 (M = Ca, Sr, Ba) binary mixtures were stirred and equilibrated at 830 °C for times sufficient to dissolve the added oxide before measuring the liquidus temperature. The cooling rate was 3 °C min^{-1} and the melt was allowed to equilibrate at about 25 °C above the liquidus temperature for at least 2 h between successive melting-point determinations. Small crystals of NaCl (< 0.005 g) were added at the expected liquidus temperature to prevent supercooling. In this way the thermal arrest (or the change in the slope of the cooling curve) could be reproduced to within ±0.3 °C, in most cases to within ±1 °C. Generally, the accuracy of the freezing-point changes was within ±0.3 °C. The composition of the melt was changed in the same way as described above. The liquidus temperature of the new composition was determined, and the oxide additions were continued until the oxide solubility limit was exceeded.

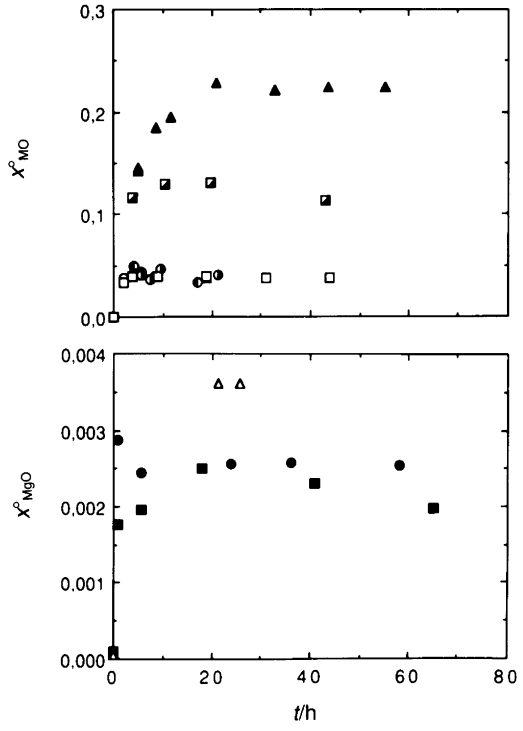

Fig. 2. Equilibration time for dissolution of MO in NaCl–MCl_2 melts. (●) $x^{\circ}_{MgCl_2}$ = 0.75, T = 730 °C; (■) $x^{\circ}_{MgCl_2}$ = 0.75, T = 830 °C; (△) $x^{\circ}_{MgCl_2}$ = 1, T = 730 °C; (○, ◐, ◑) $x^{\circ}_{CaCl_2}$ = 0.50, T = 850 °C; (□) $x^{\circ}_{SrCl_2}$ = 0.25, T = 850 °C; (◪) $x^{\circ}_{SrCl_2}$ = 0.50, T = 850 °C; (▲) $x^{\circ}_{BaCl_2}$ = 0.25, T = 850 °C.

Composition by chemical analysis of melt samples after oxide saturation. This was performed by determining the total Cl^- content by Mohr's titration, and the $x_{Na^+}/_{M^{2+}}$ ratios were found by atomic absorption spectroscopy. Precipitation of the $M_{m+n}O_nCl_{2m}$ compound was not observed in any of the melt compositions investigated.

Results and discussion

Fig. 2 shows MO concentrations as a function of dissolution time in some MCl_2–NaCl melts. The equilibration time is as long as 20 h in the $BaCl_2$ system and somewhat shorter for the other melts containing an alkaline-earth chloride. Fig. 3 shows the solubilities of alkaline-earth oxide in sodium chloride–alkaline-earth chloride melts. The results are plotted as mole fraction of dissolved MO, x°_{MO}, vs. the mole fraction of MCl_2, $x^\circ_{MCl_2}$, in the melt. This notation for the mole fractions implies that $x^\circ_{NaCl} + x^\circ_{MCl_2} + x^\circ_{MO} = 1$. Experimental results from the solubility measurements can be found in Table 1. It is evident that the solubility of alkaline-earth oxides in NaCl–MCl_2 melts increases with increasing atomic number of the alkaline-earth. Since the solubilities of these oxides in molten alkali chlorides are very low,[16,17] the observed enhanced solubilities are most probably due to oxide complex formation reactions according to eqn. (3).

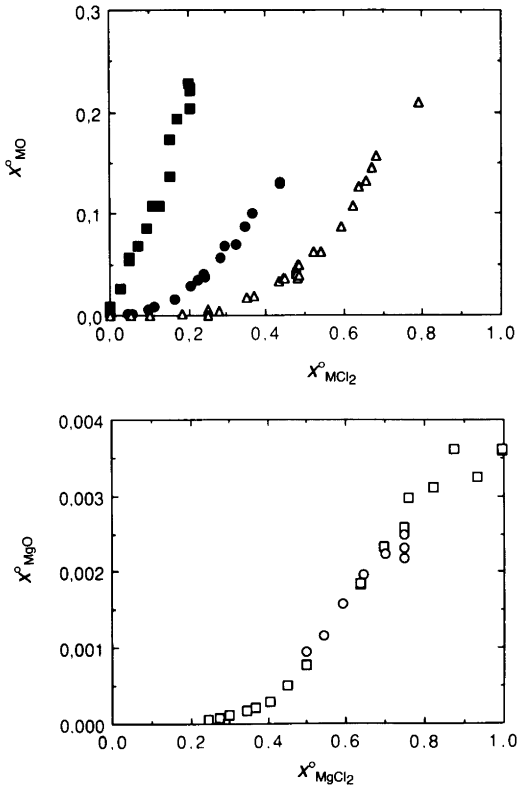

Fig. 3. Solubility of MO in NaCl–MCl_2 melts. (□) NaCl–$MgCl_2$, T = 730 °C; (○) NaCl–$MgCl_2$, T = 830 °C; (△) NaCl–$CaCl_2$, T = 850 °C; (●) NaCl–$SrCl_2$, T = 850 °C; (■) NaCl–$BaCl_2$, T = 850 °C.

Table 1. Solubilities of MO in NaCl and in MCl_2–NaCl melts. M = Mg, Ca, Sr and Ba, respectively. $x^\circ_{MCl_2} + x^\circ_{NaCl} + x'_{MO} = 1$.

$x^\circ_{MCl_2}$	x°_{MO}	$x^\circ_{MCl_2}$	x°_{MO}	$x^\circ_{MCl_2}$	x°_{MO}
$MgCl_2$, T = 730 °C					
0.247	5.2×10^{-5}	0.450	5.1×10^{-3}	0.748	2.5×10^{-3}
0.247	6.1×10^{-5}	0.500	7.7×10^{-3}	0.760	3.0×10^{-3}
0.274	8.5×10^{-5}	0.637	1.8×10^{-3}	0.820	3.1×10^{-3}
0.303	1.1×10^{-4}	0.637	1.9×10^{-3}	0.872	3.6×10^{-3}
0.344	1.8×10^{-4}	0.696	2.3×10^{-3}	0.932	3.3×10^{-3}
0.369	2.2×10^{-4}	0.748	2.6×10^{-3}	0.996	3.6×10^{-3}
0.407	2.8×10^{-4}	0.748	2.6×10^{-3}	0.996	3.6×10^{-3}
$MgCl_2$, T = 830 °C					
0.500	9.4×10^{-4}	0.644	2.0×10^{-3}	0.748	2.5×10^{-3}
0,541	1.2×10^{-3}	0.699	2.2×10^{-3}	0.748	2.3×10^{-3}
0.591	1.6×10^{-3}	0.747	2.2×10^{-3}		
$CaCl_2$, T = 850 °C					
0.000	10^{-5}	0.442	0.037	0.485	0.039
0.051	10^{-4}	0.449	0.036	0.523	0.063
0.102	0.001	0.476	0.047	0.541	0.063
0.181	0.001	0.477	0.044	0.592	0.088
0.249	10^{-4}	0.478	0.044	0.623	0.108
0.249	0.005	0.479	0.041	0.638	0.127
0.281	0.005	0.479	0.040	0.655	0.132
0.351	0.017	0.480	0.050	0.672	0.146
0.368	0.019	0.481	0.037	0.683	0.158
0.434	0.033	0.484	0.049	0.790	0.210
$SrCl_2$, T = 850 °C					
0.000	$(6\pm2)\times10^{-4}$	0.239	0.041	0.294	0.069
0.045	0.001	0.240	0.039	0.325	0.071
0.057	0.002	0.240	0.039	0.348	0.087
0.095	0.005	0.240	0.040	0.367	0.101
0.113	0.009	0.241	0.037	0.435	0.130
0.163	0.017	0.241	0.038	0.435	0.131
0.205	0.030	0.241	0.038		
0.225	0.035	0.283	0.057		
$BaCl_2$, T = 850 °C					
0.000	$(7\pm2)\times10^{-3}$	0.109	0.108	0.203	0.228
0.024	0.026	0.126	0.108	0.204	0.224
0.049	0.057	0.154	0.138	0.204	0.225
0.050	0.054	0.154	0.174	0.205	0.221
0.070	0.069	0.170	0.193		
0.095	0.085	0.203	0.203		

The NaCl–$MgCl_2$–MgO system (with or without $CaCl_2$ and $BaCl_2$)

Solubility studies. The solubility of MgO has been measured in 29 mixtures of NaCl and $MgCl_2$ in the entire concentration range at 730 and 830 °C. The results, shown in the lower part of Fig. 3 and listed in Table 1, indicate that the MgO solubility is practically zero in the composition range of the electrolyte used industrially for Mg production, ca. 7 mol % $MgCl_2$, whereas it increases in the acidic range of the NaCl–$MgCl_2$ mixture ($x^\circ_{MgCl_2} > 0.33$). A temperature change from 730 to 830 °C does not seem to affect the MgO solubility within the experimental accuracy. Ad-

ditions of $BaCl_2$ (30 mol %) or $CaCl_2$ (up to 35 mol %) in a 6.4 mol % $MgCl_2$ mixture of NaCl and $MgCl_2$ had (as shown in Fig. 4) no effect on the MgO solubility, which remained practically zero even after 60 h of equilibration time with continuous stirring. The $BaCl_2$- or $CaCl_2$-containing melts compare well with certain electrolytes used industrially for magnesium production.[15a] The reason for the low oxide solubility in these melts is explained by reaction (14). This reaction has $\Delta G^\circ << 0$ for M = Ca and Ba. The solubilities of CaO and BaO in NaCl–$CaCl_2$ and NaCl–$BaCl_2$ melts, respectively, are high as shown in Fig. 3. Since reaction (14) is shifted very much to the MgO side, however, there will be practically no MO(s) left to dissolve in $MgCl_2$–NaCl–$CaCl_2$ ($BaCl_2$) melts when $MgCl_2$(s) is added in excess.

$$MgCl_2(l,mix) + MO(s) = MCl_2(l,mix) + MgO(s) \quad (14)$$

$$MgCl_2(l) + MgO(s) = Mg_2OCl_2(l) \quad (15)$$

$$x_{Mg_2OCl_2} = K_{15}k^{-1}a_{MgCl_2} \quad (16)$$

By assuming that $m = n = 1$ for the $MgCl_2$–NaCl–MgO system, reaction (3) takes the form of reaction (15). Assuming that this reaction explains the total MgO solubility, the mole fraction of the oxide complex will, according to eqn. (6), be given by eqn. (16), where K_{15} and k are the equilibrium constant of eqn. (15) and the constant activity coefficient of Mg_2OCl_2 in the $MgCl_2$–NaCl melt, respectively. Since the solubility of MgO is very low in NaCl–$MgCl_2$ melts, we may use activity data obtained for binary NaCl–$MgCl_2$ melts[26] to make a plot of $x_{Mg_2OCl_2}$ versus a_{MgCl_2}. This is shown in Fig. 5. The two lines are obtained through a least-squares fitting of the data at low $MgCl_2$ concentrations, $x^\circ_{MgCl_2} < 0.33$, basic melts, and at high $MgCl_2$ concentrations $x^\circ_{MgCl_2} > 0.33$, acidic melts, respectively. Fitting

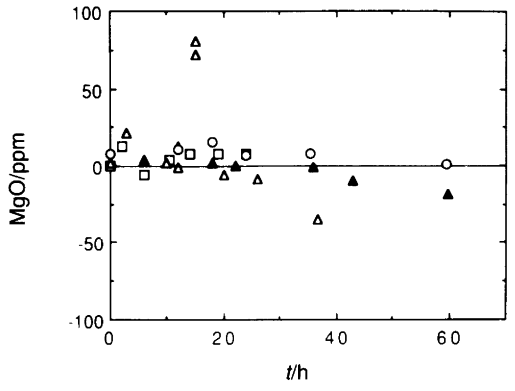

Fig. 4. MgO solubilities in a 10 wt % $MgCl_2$, 90 wt % NaCl melt with $BaCl_2$ or $CaCl_2$ added at 850 °C. (▲) 60 wt % $BaCl_2$; (□) 10 wt % $CaCl_2$; (△) 20 wt % $CaCl_2$; (○) 50 wt % $CaCl_2$.

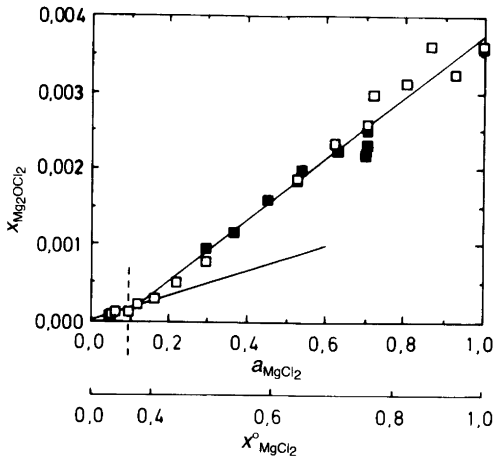

Fig. 5. Model concentrations of Mg_2OCl_2 versus a_{MgCl_2} in MgO-saturated NaCl–$MgCl_2$ melts at 730 °C (□) and 830 °C (■). Dashed line, $x_{MgCl_2} = 0.333$. Full lines are regression lines; $x_{MgCl_2} < 0.3$ and > 0.3, $r = 0.998$ and 0.977, respectively ($x_{NaCl} + x_{MgCl_2} + x_{Mg_2OCl_2} = 1$).

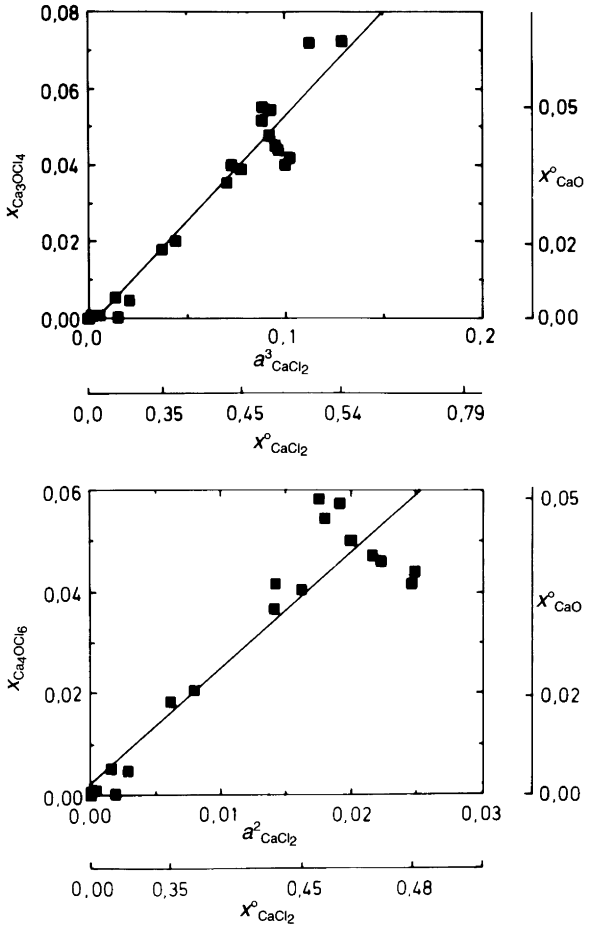

Fig. 6. Model concentrations of Ca_3OCl_4 (Ca_4OCl_6) versus $a^2_{CaCl_2}$ ($a^3_{CaCl_2}$) in CaO-saturated NaCl–$CaCl_2$ melts at 850 °C. (■) Measured; (—) regression lines, Ca_3OCl_4; $r = 0.864$, Ca_4OCl_6; $r = 0.877$ ($x_{NaCl} + x_{CaCl_2} + x_{Ca_mOCl_{2m}} = 1$).

the data with one line gives a worse fit with a smaller correlation coefficient, and the line does not pass through the origin. Since the equilibrium constant of eqn. (15) should be constant over the whole concentration range of $MgCl_2$ concentrations, owing to the very low oxide solubilities, the change in slope of the line on passing from the basic into the acidic region must be due to a change in the activity coefficient of the Mg_2OCl_2 complex. The change in this activity coefficient is not unexpected, since significant thermodynamic and structural changes occur in this melt at $x^\circ_{MgCl_2} = 0.33$.[26,27]

The above arguments do not exclude the formation of other oxide species in solution, but indicate that our assumption of the formation of the Mg_2OCl_2 complex is reasonable. This assumption is also in agreement with the data of Combes *et al.*,[16] who proposed the Mg_2O^{2+} species when MgO dissolved in $MgCl_2$–NaCl–KCl melts. Sharma[20] determined the liquidus line in MgF_2–MgO (CaO, Al_2O_3) systems. From the MgF_2 liquidus, activities of MgF_2 are calculated and compared with model activities. Sharma assumed Temkin[25] activities in solutions where the cations Mg^{2+}, Ca^{2+}, Al^{3+} and AlO^+ and the anions F^- and O^{2-} were present. The experimental data fitted reasonably well with model activities.

It is, however, not reasonable to assume that O^{2-}, Mg^{2+} and Al^{3+} can be present to a significant extent in these melts, since the solubilities of MgO and Al_2O_3 are very small in alkali halide melts, and strong coulomb interactions will occur between highly charged positive and negative ions. As shown in Table 2, the data of Sharma fit well with the following models:

1. MgF_2–MgO:

$$MgF_2(l) + MgO(s) = Mg_2O^{2+} + 2F^- \qquad (17)$$

with random mixing of Mg_2O^2 and Mg^{2+} in an F^- environment.

2. MgF_2–CaO:

$$2MgF_2(l) + CaO(s) = Mg_2O^{2+} + Ca^{2+} + 4F^- \qquad (18)$$

with random mixing of Mg_2O^{2+} and Ca^{2+} in an F^- environment.

3. MgF_2–Al_2O_3:

$$2MgF_2(l) + Al_2O_3(s) = Mg_2O^{2+} + 2AlO^+ + 4F^- \qquad (19)$$

with random mixing of the cations Mg_2O^{2+}, AlO^+ and Mg^{2+} in an F^- environment.

Table 2. Activities of MgF_2 in some binary melts based on phase-diagram data[20] compared with model activities. $\Delta H^\circ_{f,MgF_2} = 58.702$ kJ mol^{-1}.[28]

System	x_{MO}	a_{MgF_2} from phase diagram[20]	Model activities	
			a_{MgF_2}	Model
MgF_2–MgO	0.085	0.89	0.91	eqn. (17)
MgF_2–CaO	0.075	0.84	0.84	eqn. (18)
MgF_2–Al_2O_3	0.025	0.96	0.94	eqn. (19)

The NaCl–$CaCl_2$–CaO system

Solubility studies. Fig. 3 (upper part) and Table 1 give the solubilities of CaO in 30 mixtures of NaCl and $CaCl_2$ over the entire concentration range at 850 °C. The results are similar to those obtained for the NaCl–$MgCl_2$–MgO system in the sense that the solubility increases markedly with increasing concentration of $CaCl_2$ above a certain $CaCl_2$ concentration level in the melt. The solubility of CaO in pure $CaCl_2$ is exactly the same as the value reported recently by Perry and MacDonald,[29] and not far from the one given by Wenz *et al.*[19] The solubility of CaO in the KCl–$CaCl_2$ systems[29] is about 50 % of the solubilities observed in the present work for CaO in the NaCl–$CaCl_2$ system.

Several combinations of values for m and n in reaction (3) have been tested to model the present CaO solubility data. Good fits have been obtained for $m = 2$ or 3, and $n = 1$ or 2, i.e. by assuming formation of an oxide complex according to reaction (20). In Fig. 6 $x_{Ca_{m+n}O_nCl_{2m}(l)}$ is plotted versus $a^m_{CaCl_2}$ [eqn. (6)] for $m = 2$ and 3 and $n = 1$ over an oxide concentration range which is low enough to keep $x_{complex}/x_{CaCl_2} \leq 0.25$. At this low oxide concentration ($x^\circ_{CaO} < 0.05$, $m = 3$, $x^\circ_{CaO} < 0.063$, $m = 2$), the activity coefficient of the oxochloro complex ought to be constant. Furthermore, the calcium chloride activites obtained from measurements in the binary $CaCl_2$–NaCl system[26] should not be too much in error. It should again be emphasized that the present analysis cannot lead to a definite conclusion concerning the value of n, and only a value of $n = 1$ is tested.

$$mCaCl_2(l) + nCaO(s) = Ca_{m+n}O_nCl_{2m}(l) \qquad (20)$$

Cryoscopic studies. Liquidus temperatures for the NaCl–$CaCl_2$ system for $x^\circ_{NaCl} = 0.657$ when adding CaO are shown in Fig. 7. The interpretation of these results is, however, somewhat ambiguous because of the formation of a solid solution of $CaCl_2$ in NaCl(s) as reported by Seltveit and Flood.[30] The theoretical freezing points in Fig. 7 are calculated using eqns. (9) and (12), taking into consideration the solid solution data given by the available phase diagram[30] and the experimental activity data of NaCl in the above binary obtained by Østvold.[26] The activity data ob-

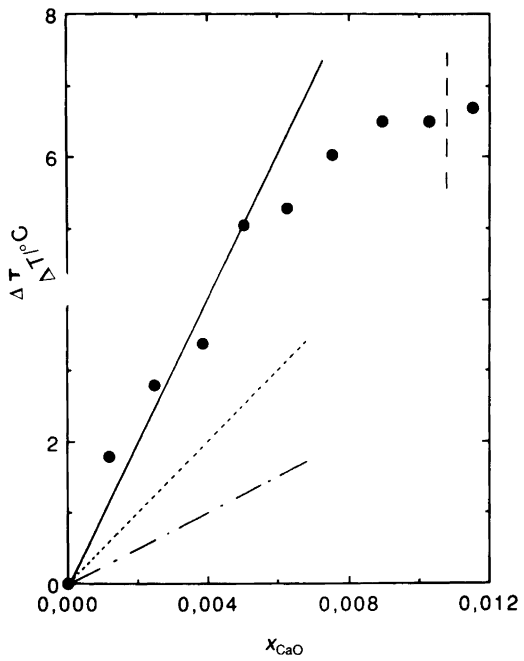

Fig. 7. Freezing-point elevations of a NaCl–$CaCl_2$ melt (x°_{NaCl} = 0.657) with CaO additions. The vertical line shows saturation of CaO at 660 °C. (●) Measured; (----) m = 2, n = 1; (——) m = 3, n = 1; (–·–) m = 2, n = 2.

tained at 850 °C were corrected to liquidus temperatures using $\Delta\bar{H}_{NaCl}$ calculated from measured binary enthalpy of mixing data.[27]

Based on the present calculations, however, Fig. 7 indicates that the oxochloro complex Ca_4OCl_6 is the predominant oxide-containing species up to oxide saturation in this binary melt. The saturation was determined by analysing a melt sample taken at 660 °C. Saturation is indicated by a vertical line in Fig. 7. Data are given in Table 3.

The NaCl–$SrCl_2$–SrO system

Solubility studies. Results concerning SrO solubility in 22 NaCl–$SrCl_2$ mixtures in the concentration range 0–50 mol % $SrCl_2$ in the $SrCl_2$–NaCl binary at 850 °C are plotted in Fig. 3 and are listed in Table 1. Furthermore, solubility data from three mixtures obtained at NaCl liquidus temperatures are given in Table 3.

By using the same procedure as before, we tested several combinations of values for m and n, obtaining good fits for various pairs of values. As shown by our cryoscopic results for the NaCl–$SrCl_2$–SrO system discussed below, the (m = 3, n = 1) and (m = 2, n = 1) pairs both seem to give a relative good fit to our cryoscopic and solubility data. Reaction (21), with m = 2 and 3, may therefore explain the solubility data as shown in Fig. 8, where $x_{Sr_{m+1}OCl_{2m}}$ is plotted versus $a^m_{SrCl_2}$ for m = 2 and 3 according to eqn. (22). Fig. 8 shows a linear relationship between $x_{Sr_{m+1}OCl_{2m}}$ and $a^m_{SrCl_2}$ (m = 2 and 3) over a 0–1.7 mol % oxide concentration range where $x_{complex}/x_{SrCl_2} \leq 0.25$. As long as the oxide concentration is small, the activity coefficient of the oxochloro complex may still be constant. At the same time the mole fraction of $SrCl_2$ will be considerably higher than the complex mole fraction, and a calculation of the $SrCl_2$ activity from the NaCl–$SrCl_2$ binary may not be too much in error.

$$m SrCl_2(l) + SrO(s) = Sr_{m+1}OCl_{2m} \quad (21)$$

$$x_{Sr_{m+1}OCl_{2m}} = K_{21}k^{-1}a^m_{SrCl_2} \quad (22)$$

Cryoscopic studies. Cryoscopic results for additions of SrO to the composition range of the NaCl–$SrCl_2$ binary where NaCl crystallizes on cooling are shown in Figs. 9–11. When adding SrO to the binary chloride melts an elevation of the liquidus temperature is observed. Using eqns. (9) and (12) and different values of m and n theoretical freezing points can be calculated. The activity data given by Østvold were corrected to liquidus temperatures using calculated ΔH_{NaCl} data based on the measurements of Østvold.[27] SrO saturation at the temperatures slightly above the highest liquidus temperatures, indicated by vertical dotted lines in Figs. 9–11, was confirmed by chemical analysis.

Table 3. MO solubilites just above the ternary liquidus temperatures in MO–MCl_2–NaCl melts compared with solubilities obtained at 850 °C. $x^\circ_{MCl_2} + x^\circ_{NaCl} + x^\circ_{MO} = 1$.

System	$x^\circ_{MCl_2}$	T_f (ternary)/°C	T (sample)/°C	x_{MO}(satd.) at T(sample)	x_{MO}(satd.) at 850 °C[a]
NaCl–$CaCl_2$	0.343	634	660	0.011	0.014
NaCl–$SrCl_2$	0.119	762	770	0.008	0.009
	0.195	735	740	0.023	0.026
	0.285	722	760	0.047	0.056
NaCl–$BaCl_2$	0.092	777	783	0.080	0.090
	0.169	759	768	0.165	0.190

[a]Interpolated.

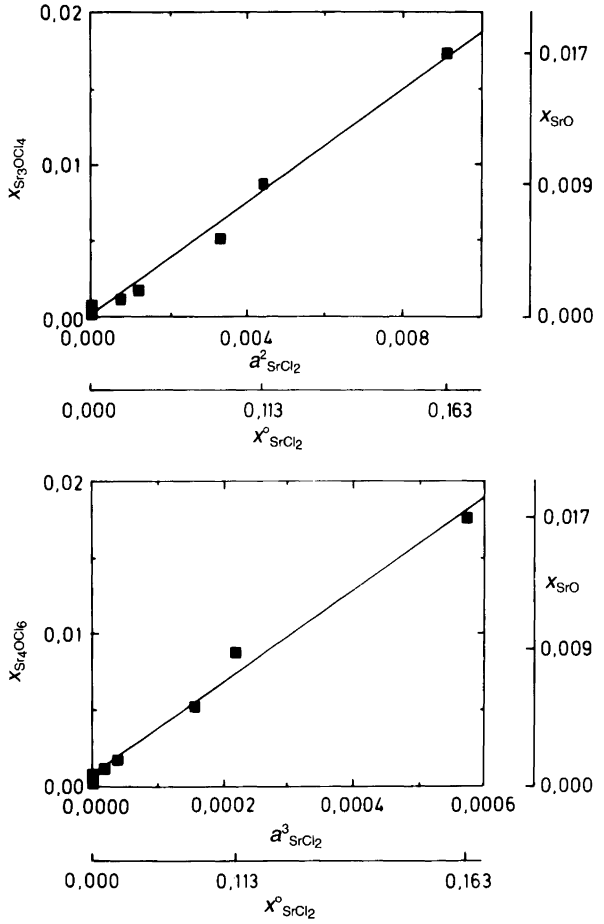

Fig. 8. Model concentrations of Sr_3OCl_4 (Sr_4OCl_6) versus $a^2_{SrCl_2}$ ($a^3_{SrCl_2}$) in SrO-saturated NaCl–$SrCl_2$ melts at 850 °C. (■) Measured; (——) regression lines, Sr_3OCl_4; r = 0.988, Sr_4OC_6; r = 0.989 ($x_{NaCl} + x_{SrCl_2} + x_{Sr_mOCl_{2m}} = 1$).

Saturation occurs when the freezing points become independent of the addition of SrO. The SrO saturation concentration was determined by analysing samples taken from the melts at T = 770, 740 and 760 °C for the $x^\circ_{SrCl_2}$ = 0.12, 0.20 and 0.29 melts, respectively. Data are given in Table 3. Figs. 9–11 indicate that it seems reasonable to believe that both the Sr_3OCl_4 and Sr_4OCl_6 compounds may form in these melts.

The NaCl–$BaCl_2$–BaO system

Solubility studies. The solubilities of BaO in 16 NaCl–$BaCl_2$ mixtures in the 0–31 mol % $BaCl_2$ concentration range at 850 °C are plotted in Fig. 3 and listed in Table 1. Furthermore, results from two mixtures obtained at NaCl liquidus temperatures are given in Table 3. As shown in Fig. 3, there seems to be an approximate 1:1 relationship between the number of dissolved moles of BaO and the number of moles of $BaCl_2$ in the NaCl–$BaCl_2$ mixture. This observation leads to the conclusion that reactions such as reaction (23) take place in this system.

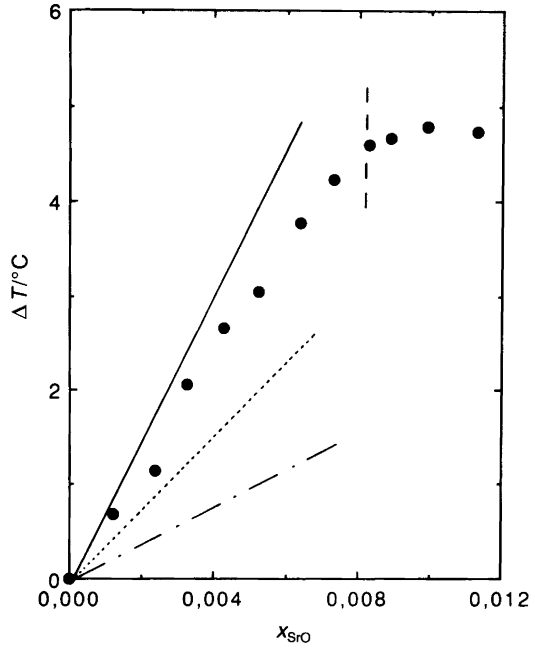

Fig. 9. Freezing-point elevations of an NaCl–$SrCl_2$ melt (x°_{NaCl} = 0.88) with SrO additions. The vertical line shows the saturation of SrO at 770 °C. (●) Measured; (····) m = 2, n = 1; (——) m = 3, n = 1; (–·–) m = 2, n = 2.

$$m\mathrm{BaCl_2(l)} + m\mathrm{BaO(s)} = \mathrm{Ba_{2m}O_mCl_{2m}(l)} \qquad (23)$$

Given the assumption used throughout this work, namely that all the dissolved alkaline-earth oxide is used

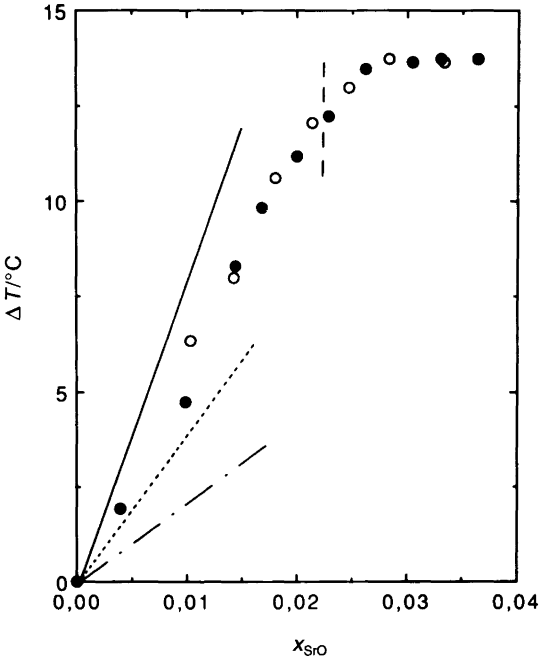

Fig. 10. Freezing-point elevations of an NaCl–$SrCl_2$ melt (x°_{NaCl} = 0.80) with SrO additions. The vertical line shows the saturation of SrO at 740 °C. (○, ●) Measured; (····)m = 2, n = 1; (——) m = 3, n = 1; (–·–) m = 2, n = 2.

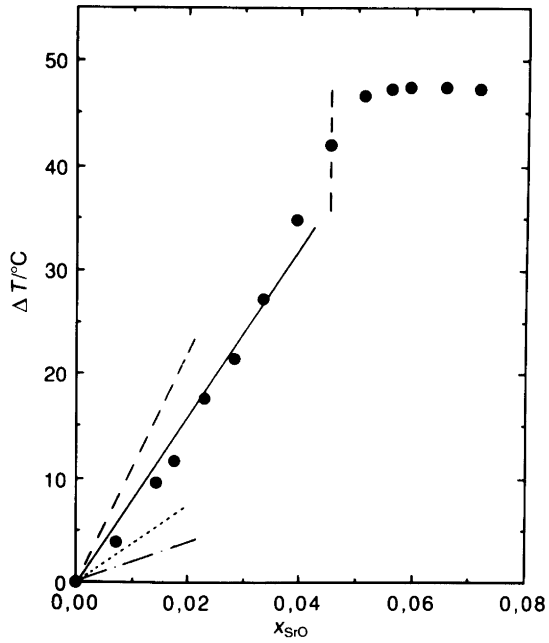

Fig. 11. Freezing-point elevations of an NaCl–$SrCl_2$ melt (x°_{NaCl} = 0.70) with SrO additions. The vertical line shows the saturation of SrO at 760 °C. (●) Measured; (····) m = 2, n = 1; (——) m = 3, n = 1; (– – –) m = 4, n = 1; (–·–) m = 2, n = 2.

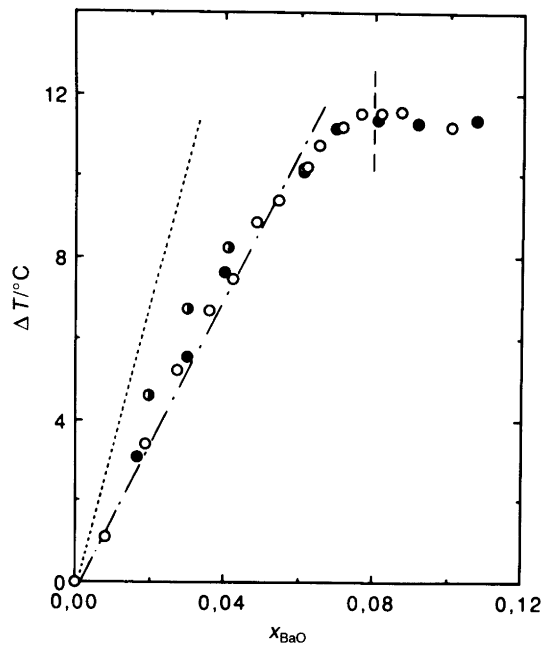

Fig. 12. Freezing-point elevations of an NaCl–$BaCl_2$ melt (x°_{NaCl} = 0.90) with BaO additions. The vertical line shows the saturation of BaO at 783 °C. (●, ○, ◑) Measured; (····) m = 2, n = 1; (–·–) m = 2, n = 2.

for oxide complex formation, eqn. (23) implies that there would be little $BaCl_2$ left at equilibrium. A plot based on eqn. (6) is therefore difficult to obtain in the present case, and a value for m cannot be estimated on the basis of the solubility data.

Cryoscopic studies. Liquidus temperatures when adding BaO to binary NaCl–$BaCl_2$ melts in which NaCl crystallizes on cooling are shown in Figs. 12 and 13. An elevation of the liquidus temperatures with increasing BaO content is observed. Ideal Temkin mixtures are observed for the NaCl–$BaCl_2$ binary,[26] and introducing ideal Temkin activities for NaCl in the ternary mixtures should not introduce significant errors as long as the BaO contents are relatively small. Based on this assumption the theoretical freezing points are calculated using eqns. (9) and (12) as before.

The experimental liquidus temperatures given in Figs. 12 and 13 indicate Ba_3OCl_4 and $Ba_4O_2Cl_4$ species in the melt up to BaO saturation. As can be observed from Fig. 13, Ba_3OCl_4 may be formed in $BaCl_2$-rich melts, while reactions (24) and (25) take over at higher oxide additions, giving a melt at saturation at which $BaCl_2$ is consumed. The BaO saturation concentration, indicated by vertical dotted lines in Figs. 12 and 13, was determined from samples taken at T = 783 and 768 °C for initial mole fractions of $BaCl_2$ equal to 0.10 and 0.20 melts, respectively. Results are given in Table 3.

$$Ba_3OCl_4 + BaO = Ba_4O_2Cl_4 \quad (24)$$

$$2BaCl_2 + 2BaO = Ba_4O_2Cl_4 \quad (25)$$

Structural interpretations. The charge per unit surface area of the alkaline-earth metal ions shown in Table 4 increases in the sequence Ba^{2+}–Sr^{2+}–Ca^{2+}–Mg^{2+}. We believe that the resultant change in coulomb interaction between the alka-

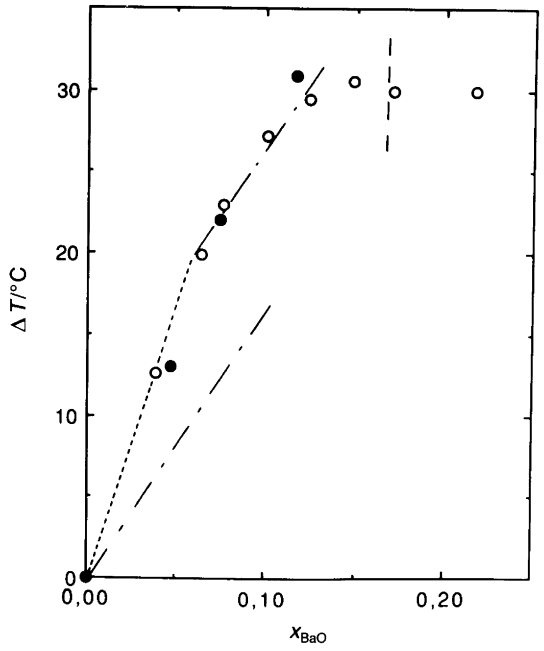

Fig. 13. Freezing-point elevations of an NaCl–$BaCl_2$ melt (x°_{NaCl} = 0.80) with BaO additions. The vertical line shows the saturation of BaO at 768 °C. (○, ●) Measured; (····) m = 2, n = 1; (–·–) m = 2, n = 2.

Table 4. Charge per surface area of alkaline-earth ions.

Ion	Radius/10^{-8} cm	$[2/(4/3)\pi r^3]/10^{-24}$ cm^3
Mg^{2+}	0.72	1.28
Ca^{2+}	0.99	0.49
Sr^{2+}	1.12	0.34
Ba^{2+}	1.36	0.19

line-earth ion and the oxygen ion has a strong influence on the M–O–Cl complexing observed in the present melts. Our experimental data indicate formation of the Mg_2OCl_2 compound. Owing to the strong field strength of the Mg^{2+} ion, two ions are sufficient to shield the O^{2-} ion, and the $Mg_2OCl_4^{2-}$ complex with the possible structure I may form.

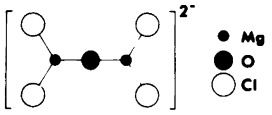

I

Since there is a considerable reduction in surface charge on going from Mg^{2+} to Ca^{2+}, we would expect a larger number of Ca^{2+} ions around each O^{2-}. Both solubility and freezing point depression data indicate Ca_3OCl_4 or Ca_4OCl_6 formation, in agreement with this expectation. Reasonable ionic species may be II and III. The change in charge per surface area on going from Ca^{2+} to Sr^{2+} is not very large, hence the same complexes as formed in the $CaCl_2$ system are expected. The tendency to form the $Sr_4OCl_8^{2-}$ ion seems, furthermore, to be enhanced in melts with high $SrCl_2$ concentrations (Fig. 10), as expected.

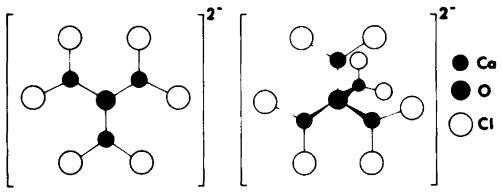

II III

In the solid phase of the system $SrCl_2$–SrO the compound Sr_4OCl_6, with hexagonal symmetry, has been detected,[31] and the solid compound Ba_4OCl_6, with O^{2-} tetrahedrally surrounded by Ba^{2+}, has been synthesized.[32] The occurrence of the abovementioned complex ions in the liquid phase is therefore not totally unexpected. When Ba^{2+} substitutes Sr^{2+} there is again a small change in surface charge, and no major structural change of the alkaline-earth oxochloro complex is expected. The cryoscopic measurements indicate Ba_3OCl_4 and $Ba_4O_2Cl_4$ compound formation, which again points towards O^{2-} ions with Ba^{2+} neighbours according to the possible ionic structures IV and V. $Ba_4O_2Cl_6^{2-}$ is obtained from $Ba_3OCl_6^{2-}$ by simple addition of one BaO unit. Each O^{2-} is surrounded by three Ba^{2+} in both structures, and there is a sharing of two triangles in the $Ba_4O_2Cl_6^{2-}$ complex. $Ba_3OCl_6^{2-}$ seems to be more stable than $Ba_4O_2Cl_6^{2-}$ in $BaCl_2$-rich melts, which is reasonable in view of the stoichiometry of the complex.

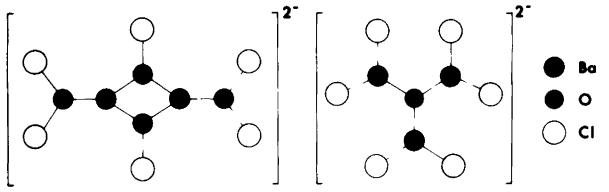

IV V

Solubility products of the alkaline-earth oxides. The solubility product of the alkaline-earth oxides in NaCl may be calculated from thermodynamic data of the pure components and binary systems.[33] By combining eqns. (26)–(28) we obtain the solubilization reaction for MO(s) in NaCl(l), eqn. (29). $\Delta G°$ is the standard Gibbs energy change for a

$$MO(s) + 2NaCl(l) = MCl_2(l) + Na_2O(l) \quad (26)$$

$$MCl_2(l) = MCl_2(l), \text{ in NaCl}) \quad (27)$$

$$Na_2O(l) = Na_2O(l, \text{ in NaCl}) \quad (28)$$

$$MO(s) + 2NaCl(l) = MCl_2(l, \text{ in NaCl}) + Na_2O(l, \text{ in NaCl}) \quad (29)$$

$$\Delta G°[\text{eqn. (29)}] - RT \ln K[\text{eqn. (29)}] = \Delta G°[\text{eqn. (26)}] + \Delta G^*[\text{eqn. (27)}] + \Delta G^*[\text{eqn. (28)}] \quad (30)$$

reaction between pure components and ΔG^* is the standard Gibbs energy change for a reaction with different standard states for reactants and products. When we choose pure components as standard states for the reactants in eqns. (27)–(29) and Henrian standard states for the dissolved species, we obtain eqn. (31) at equilibrium, in which γ_i^R is the Raoultian activity coefficient of component i in liquid NaCl.

Stern[34] has measured the Raoultian activity coefficient of Na_2O in NaCl. He gives $\gamma^R_{Na_2O} = 1.07\times10^{-4}$ in dilute solutions at 1100 K. From data given by Østvold[27] on the activities of NaCl in the binary mixtures NaCl–$MgCl_2$ ($CaCl_2$, $SrCl_2$ and $BaCl_2$), $\gamma^R_{MCl_2}$ in liquid NaCl may be obtained. Values are given in Table 5. Using these activity coefficients and the Gibbs energies of the pure components given in JANAF, we obtain K_{sp}(MO) in liquid NaCl for the different alkaline-earth oxides. The calculated solubility

Table 5. Limiting Raoultian activity coefficients of MCl_2 (mole fraction basis) at 850 °C in liquid NaCl;[26] $\lim \gamma^R_{MCl_2}$ when $x_{MCl_2} \rightarrow 0$.

Melt	$\lim \gamma^R_{MCl_2}$ $x_{MCl_2} \rightarrow 0$	$\lim RT \ln \gamma^R_{MCl_2}$/kJ mol^{-1} $x_{MCl_2} \rightarrow 0$
NaCl–$MgCl_2$	0.05	−28.0
NaCl–$CaCl_2$	0.2	−15.0
NaCl–$SrCl_2$	0.5	−6.5
NaCl–$BaCl_2$	1.0	0

products are given in Table 6, together with published solubility products obtained experimentally. Except for SrO and BaO, reasonable agreement is observed.

$$-RT \ln K_{sp}(MO) = -RT \ln x_{M^{2+}} x_{O^{2-}}$$

$$= \Delta G^\circ[\text{eqn. (26)}] + \lim_{x_{MCl_2} \rightarrow 0} RT \ln \gamma^R_{MCl_2} + \lim_{x_{Na_2O} \rightarrow 0} RT \ln \gamma^R_{Na_2O} \quad (31)$$

In Table 6 complex constants for reactions such as reaction (32), divided by the Raoultian activity coefficient of the different oxochloro compounds, are also given. Large and decreasing values in the sequence Mg^{2+}–Ca^{2+}–Sr^{2+} are observed. For the $BaCl_2$ system solubility data show that each BaO added needs one $BaCl_2$ to dissolve. We cannot therefore use eqn. (5) to calculate K_3k^{-1} for the $BaCl_2$ system from the solubility data, and only a value >> 1 for the complex constant can be suggested.

$$(m+1)M^{2+} + O^{2-} + 2mCl^- = M_{m+1}OCl_{2m} \quad (32)$$

Conclusions

The solubilities of alkaline-earth oxides in sodium chloride–alkaline-earth chloride molten mixtures have been measured and have been found to increase considerably with increasing atomic number of the alkaline earth. The measured solubility values are much larger than those previously reported in pure NaCl melts. The enhanced solubilities observed in the present work are due to complex formation. A combination of solubility and cryoscopic measurements gives a better background for the determination of the stoichiometry of the oxochloro complexes than solubility measurements alone. The present results indicate that the dominating oxide-containing complexes in alkali–alkaline-earth chloride melts have the following M/O ratios: Mg_2O, Ca_3O, Ca_4O, Sr_3O, Sr_4O, Ba_3O and Ba_4O_2.

Acknowledgements. J. Olsen carried out cryoscopic measurements in the NaCl–$CaCl_2$ system. The present work has been supported economically by Norsk Hydro and NTNF.

Table 6. Solubility products for alkaline-earth oxides in NaCl at 850 °C and complex constants for the different possible oxochloro compounds formed when MO dissolves in MCl_2–NaCl melts, divided by the Raoultian activity coefficient of these oxochloro compounds.

Oxide	$K_{sp,\ eqn.\ (31)}$	$K_{sp,\ obs}$	Compound	"Complex constant", $K_{eqn.\ (32)}k^{-1}$
MgO	7×10^{13}	5.3×10^{12} (Ref. 16)[a]	Mg_2OCl_2	2×10^9
CaO	5×10^{-8}	4.4×10^{-8} (Ref. 17)	Ca_4OCl_6	5×10^7
			Ca_3OCl_4	10^7
SrO	3×10^{-5}	7.8×10^{-8} (Ref. 17)	Sr_4OCl_6	10^6
			Sr_3OCl_4	6×10^4
BaO	9×10^{-3}	1.4×10^{-4} (Ref. 17)	$Ba_4O_2Cl_4$	>>1

[a]Determined in molten equimolar NaCl–KCl at 730 °C.

We also want to express our gratitude to O. Wallevik, Norsk Hydro, for valuable discussions.

References

1. Grjotheim, K., Holm, J. L., Lillebuen, B. and Øye, H. A. *Trans. Faraday Soc. 67* (1971) 640.
2. Berge, B., Holm, J. L. and Lillebuen, B. *Acta Chem. Scand. 26* (1972) 257.
3. Grjotheim, K., Nikolic, R. and Øye, H. A. *Acta Chem. Scand. 24* (1970) 489.
4. Dumas, D., Fjeld, K., Grjotheim, K. and Øye, H. A. *Acta Chem. Scand. 27* (1973) 319.
5. Grjotheim, K., Holm, J. L., Lillebuen, B. and Øye, H. A. *Acta Chem. Scand. 26* (1972) 2050.
6. Grjotheim, K., Schultz, A. H. and Øye, H. A. *Metallurgica 26* (1972) 236.
7. Schultz, A. H. and Øye, H. A. *Metallurgica 27* (1973) 252.
8. Wypartowicz, J., Østvold, T. and Øye, H. A. *Electrochim. Acta 25* (1980) 151.
9. Østvold, T. and Øye, H. A. *Light Metals 1980,* 109th AIME Annual Meeting, Las Vegas, NE 1980, p. 937.
10. Aarebrot, E., Andersen, R. E., Østvold, T. and Øye, H. A. *Light Metals 1977,* 106th AIME Annual Meeting, Atlanta, GA 1977, p. 491.
11. Aarebrot, E., Andersen, R. E., Østvold, T. and Øye, H. A. *Metallurgica 32* (1977) 41.
12. Nakajima, T., *Ph. D. Thesis,* Kyoto University, Kyoto, Japan 1975.
13. Martin, R. L. and Wesi, J. B. *J. Inorg. Nucl. Chem. 24* (1962) 105.
14. Inyushkina, T. L., Petukhova, L. P. and Kornilova, V. T. *Russ. J. Inorg. Chem. 20* (1975) 594.
15. Strelets, K. L. *Electrolytic Production of Magnesium,* Veder, Jerusalem 1977; (a) p. 232; (b) pp. 243–247.
16. Combes, R., Andrade, F. de, Barros, A. de and Ferreira, H. *Electrochim. Acta 25* (1980) 371.
17. Naumann, von D. and Reinhard, G. *Z. Anorg. Allg. Chem. 343* (1966) 165.
18. Neumann, B., Kroeger, C. and Juettner, H. *Z. Elektrochem. 41* (1935) 729.
19. Wenz, D. A., Johnson, I. and Wolson, R. D. *J. Chem. Eng. Data 14* (1969) 252.
20. Sharma, R. A. *J. Am. Ceram. Soc. 71* (1988) 272.
21. Førland, T. and Ratkje, S. K. *Acta Chem. Scand. 27* (1973) 1883.
22. Ratkje, S. K. *Electrochim. Acta 21* (1976) 515.

23. Ratkje, S. K. and Førland, T. *T. Archiwum Hutnictwa 22* (1977) 159.
24. Dawson, R., Brackett, E. B. and Brackett, T. E. *J. Phys. Chem. 67* (1963) 1669.
25. Temkin, M. *Acta Physicochim. URSS 20* (1945) 41.
26. Østvold, T. *J. High Temp. Sci. 4* (1972) 51.
27. Østvold, T. *J. Phys. Chem. 76* (1972) 1616.
28. Chase, M. W., Jr., Davies, C. A., Dourney, J. R., Jr., Frurip, D. J., McDonald, R. A. and Syverud, A. N. JANAF Thermochemical Tables, 3rd ed., 1985, Vol. 14, p. 107.
29. Perry, G. and McDonald, L. G. *J. Nucl. Mat. 130* (1985) 234.
30. Seltveit, A. and Flood, H. *Acta Chem. Scand. 12* (1958) 1030.
31. Frit, B., Clibany, M. M., Tanguy, B. and Hagenmuller, P. *Bull. Soc. Chim. Fr. 35* (1968) 127.
32. Frit, B., Holmberg, B. and Galy, J. *J. Acta Crystallogr., Sect. B 26* (1970) 16.
33. Kucera, G. H. and Saboungi, M. L. *Met. Trans. B 7* (1976) 213.
34. Stern, K. H. *Electrochim. Acta 24* (1979) 509.

Received May 22, 1990.